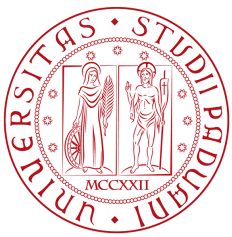


Physics laboratory -LM, A.A. 2021/22
Group: *5*
Cohort: *1*
Experience date: *10-13-14/12/2021*
Delivery date: *23-12-2021*

Giovanni Celotto	2052372	giovanni.celotto@studenti.unipd.it
Andrea Pompermaier	2053046	andrea.pompermaier@studenti.unipd.it
Massimo Colombo	2056104	massimo.colombo@studenti.unipd.it
Cristian Tibambre	2054971	cristiandavid.tibambreheredia@studenti.unipd.it

Timing

1 Introduction

Time measurements play a key role in many physical experiments. For this reason, the optimization of timing resolution is fundamental to obtain accurate estimations of time intervals. An important device in many experimental electronics is the Constant Fraction Timing Discriminator (CFTD) that provides a time marker at the optimum fraction of the amplitude of an incoming signal. It works by doubling the input into two signals, one is attenuated by a constant factor while the other is inverted and delayed by a percentage of the rising time. With the optimal combination of these two factors, it is possible to reduce the dependence of the time pick-off on the energy of the analyzed events and it is thus possible to improve the resolution of the time measurement. Another important module is the Time to Amplitude Converter (TAC), necessary to measure the time difference between two signals. Through the TAC it is possible to optimize the temporal resolution by varying some appropriate variables that characterize both the detectors and the CFTD.

2 Objectives

The purposes of this experiment are:

- Energy calibration of the organic scintillators through the analysis of the Compton edge;
- Time calibration of the TAC and measurement of the delay of some LEMO wires;
- Study of the time resolution of TAC as a function of both the external delay of CFTD and the energy of the events;
- Reproduce the operation of the CFTD using a waveforms analysis algorithm and comparison of the timing results of the digital CFTD with that obtained through the analogue one;
- Measurement of the speed of light;

3 Experimental setup

The experimental setup for this experiment consists of:

- A ^{22}Na and a ^{60}Co γ-ray sources that can be positioned inside a properly shaped lead brick.
- Two cylindrical organic scintillators EJ-228 (called D1 and D2) with a 5cm diameter and 5cm thickness. They can be moved along a metal bar with a length of about 2m.
- Two Photonics Photomultipliers XP2020 with voltage divider (mod. VD124K/T).
- A digitizer CAEN (mod. DT5751) with sampling rate 1Gs/s and a resolution of 10 bit.
- An oscilloscope TEXTRONIX (mod. TBS11002C).
- Nuclear Instrument Modules (NIMs) formed by: a Power Supply (CAEN N1471); a Quad Linear Gate FAN-IN-FAN-OUT (Philips 744); a Quad Logic Unit CAEN (mod. N455) which provides the TRG IN for the digitizer; a Delay Unit; a TAC; a CFD ORTEC (mod. 395) with:
  - Signal acceptance from 0 to -10V;
  - Adjustable threshold from -10mV to -1000mV;
  - Internal delay that can be set through an external cable;
  - A potentiometer for Walk Adjustment (Z) to optimize the zero-crossing point.
- LEMO cables with different lengths and delays.
- A computer which uses VERDI acquisition system.

4 Preliminary operations

The ^{22}Na γ-ray source has been placed inside the lead collimator which directs the beam toward the two detectors. The anode signal coming from the photomultipliers is sent to the Quad Linear Gate FAN-IN-FAN-OUT where it can be split. One of the outputs was connected to the digitizer (ch0 for D1 and ch1 for D2) instead the other was connected to the CFTD. We analyzed the characteristics of the anode signal of both the detectors by using the oscilloscope. The signals are negative and they have typically a rise time of $\sim 6ns$, a fall time of $\sim 8ns$ while the amplitude has a maximum value of $\sim 1V$ (for the events near the Compton edge of the 1274keV photons). Then we set the threshold of the CFTDs at the minimum value necessary to cut off the electronic noise. Since we are typically interested in the coincidences between the signals recorded by both the detectors, we connected the outputs of the CFTDs to the Logic Unit, where it is possible to set AND or OR coincidence modes. The output signals of the CFTDs have typically a width of $\sim 150ns$ and we verified that in AND mode the signals had some timing overlap: the output of the Coincidence Unit has been taken as TRG IN of the digitizer. In order to better visualize the time distribution, we need to apply a certain delay through the Delay Unit. We connected the output of CFTD for D1 to the START of the TAC, while the output of the CFTD for D2 to the Delay Unit and then to the STOP of the TAC: the timing distribution of the TAC is recorded in the ch2 of the digitizer.

4.1 Energy calibration of the detectors

The energy recorded by the detectors is proportional to the ionized charges induced by the photon interactions. In particular, the organic scintillators used in this experience are made up of light elements (such as Carbon and Hydrogen) and the photoelectric cross section, for the range energy of interest for this experiment, is negligible with respect to that of Compton scattering. Moreover, the total absorption of a photon through multiple Compton scatterings is negligible too, so the principal processes of interaction turn out to be individual Compton scatterings. As a

consequence, the experimental spectra don't present the typical full-energy peaks but continuous distributions that end with the Compton edge. We need to use for the energy calibration the reference energy value of the Compton edge E_{CE}, which can be theoretically calculated with the following formula:

$$E_{CE} = \frac{2E_\gamma^2}{m_e c^2 + 2E_\gamma} \tag{1}$$

where E_γ is the energy of the incident photon and m_e is the electron mass.
Although the theoretical value of the Compton edge is known, in practice, due to the finite resolution of the detectors, its position can change in the experimental spectrum. In order to obtain the correct value of the energy of the experimental Compton edge, we had to analyze the relation between the resolution of the detector and the position of the peak. This analysis has been carried out through a Monte Carlo simulation of the predicted experimental distribution [1].
We started with the probability distribution of the scattered electron energy E which is given by the following expression of the Klein-Nishina formula [2]:

$$\frac{d\sigma}{dE} = \frac{\pi r_e^2}{m_e c^2 \alpha^2}\left[2 + \frac{E^2}{\alpha^2(E_\gamma - E)^2} + \frac{E}{(E_\gamma - E)}\left(\frac{E}{E_\gamma} - \frac{2}{\alpha}\right)\right] \tag{2}$$

where E_γ is the energy of the incident photon, r_e is the classical electron radius and $\alpha = \frac{E_\gamma}{m_e c^2}$.
For each event produced with a certain energy E, the experimental energy $\bar{E}$ recorded by the detectors can be obtained through a Gaussian probability distribution with a fixed resolution σ_{res} [3]:

$$p(\bar{E}) = \frac{1}{\sqrt{2\pi\sigma_{res}^2}} e^{-\frac{(\bar{E}-E)^2}{2\sigma_{res}^2}} \tag{3}$$

where σ_{res} is the detector resolution of the Compton edge (which doesn't take into account the energy dependence). This procedure has been used to simulate both Compton edges (511 keV and 1274keV) changing the parameter σ_{res}. For each simulation, we fitted the right tail of the Compton Edge (in a suitable range) using a Gaussian function in order to obtain $\zeta = \frac{\sigma}{\mu}$ (where σ and μ are the standard deviation and centroid respectively obtained by the fit). For each Compton edge, we made a linear fit of the parameter ζ as function of the σ_{res} used (Fig. 2 Fig. 3).

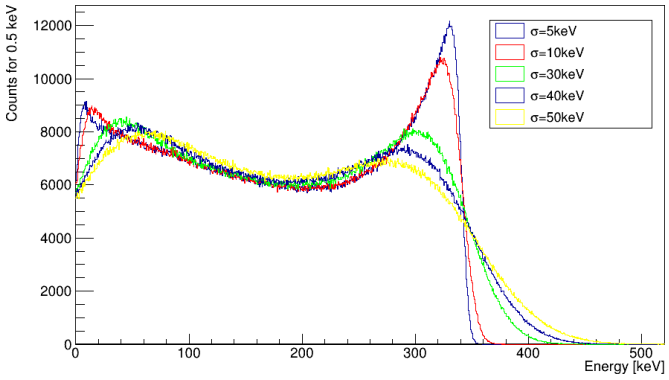

Figure 1: Simulation of Compton scattered events with different Gaussian smearing pulse resolutions for 511keV photons.

With a similar procedure, the experimental ζ_{exp} has been estimated starting from the acquired spectra. This result allows obtaining the experimental σ_{res} of each Compton edge.
Finally, we estimated the energies of the Compton edges with the experimental detector resolutions: these values have been used for the energy calibration of the two scintillators (Fig. 4, Fig. 5).

[1] N. Kudomi,"Energy calibration of plastic scintillators for low energy electrons by using Compton scatterings of γ rays",Nuclear Instruments and Methods in physics research, sec.A, 1999.
[2] Klein, O., Nishina, Y., 1929. Z. Phys. 52, 853.
[3] This process tries to model the probability distribution of the charges induced by ionization.

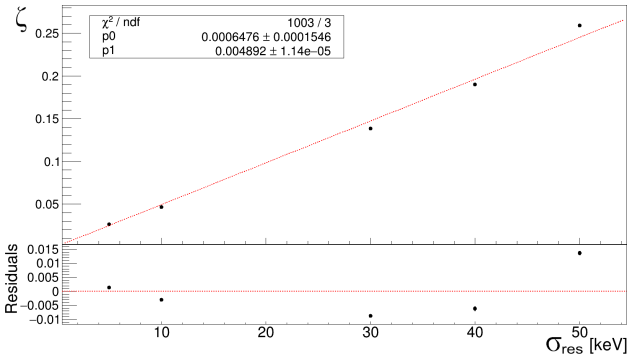

Figure 2: Linear fit of ζ as function of σ_{res} for 511 keV photons.

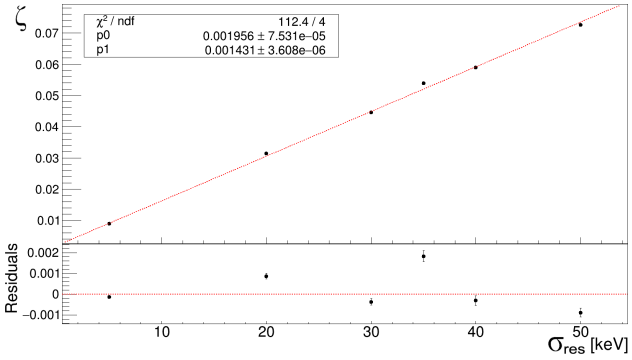

Figure 3: Linear fit of ζ as function of σ_{res} for 1275 keV photons.

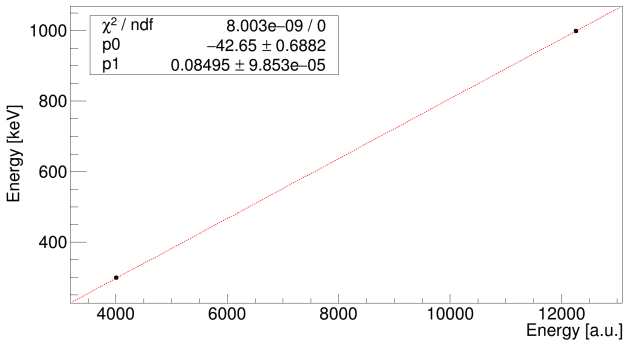

Figure 4: Calibration fit results of detector D1.

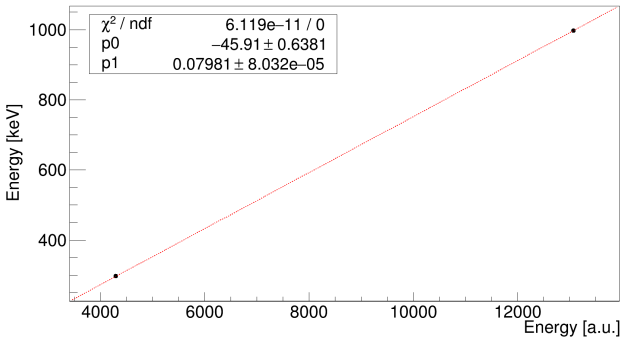

Figure 5: Calibration fit results of detector D2.

	511 keV					1275 keV				
Detector	μ_{exp} [a.u.]	σ_{exp} [a.u.]	ζ_{exp}	σ_{res} [keV]	μ_{mc} [keV]	μ_{exp} [a.u.]	σ_{exp} [a.u.]	ζ_{exp}	σ_{res} [keV]	μ_{mc} [keV]
D_1	4009 ± 3	632 ± 4	0.157 ± 0.001	31.96	298.0 ± 0.3	12260 ± 6	822 ± 4	$(6.71 \pm 0.03) \cdot 10^{-2}$	45.52	998.8 ± 0.5
D_2	4288 ± 4	692 ± 5	0.161 ± 0.001	32.78	296.3 ± 0.2	13073 ± 6	849 ± 4	$(6.49 \pm 0.03) \cdot 10^{-2}$	43.98	997.5 ± 0.4
Interpolation parameters	D_1: $p_0 = (-42.7 \pm 0.7) keV$, $p_1 = (0.0849 \pm 0.0001) keV/a.u.$					D_2: $p_0 = (-45.9 \pm 0.6) keV$, $p_1 = (0.0798 \pm 0.0001) keV/a.u.$				

Table 1: Results of the energy calibration of the detectors.

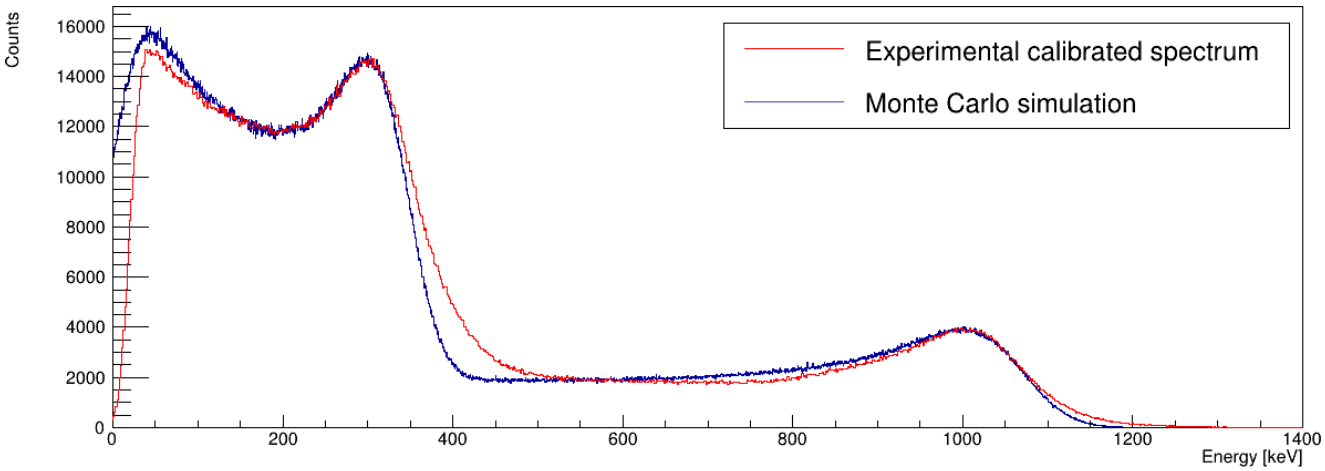

Figure 6: Comparison between the experimental spectrum and the simulated one for detector D1.

Finally, we performed a simulation of the complete spectrum in order to see the goodness of this approach (Fig. 6). To do this, it has been adjusted the ratio between the events of the first Compton edge with respect to the second one of the simulations (which takes into account the

relative efficiency and the different percentage of emitted 511 keV and 1274 keV photons), in order to correctly reproduce the experimental distribution. The results show a little discrepancy on the right tails of the Compton edges due to an underestimation of the σ_{res} through the Gaussian fit: a more precise way to carry out this type of analysis consists in an optimization of the detector resolution through the method of χ^2-minimization.

4.2 Calibration of the TAC

We proceeded by calibrating the TAC spectrum obtained in ch2. For this scope, we have acquired different spectra with different delay times (that can be selected through the multiple switches of the Delay Unit) in the range from 13 ns to 30 ns. Each spectrum has been acquired for about 3 minutes in order to have enough statistics while the two detectors were connected to the Logic Unit with the AND mode. The spectra obtained in this way are not exactly Gaussian distributions since, due to the operation of CFTD, the resolution depends on the energy of the events (see Sec. 5). However, these distributions can be approximated to Gaussians, if consider a suitable fit range around the centroid. Therefore, from the fits, we obtained the mean μ and the standard deviation σ of each sample expressed in arbitrary units (Tab. 2). Then we extracted the time calibration parameters of the TAC by making a linear fit (Fig. 7) of the delay time measured in arbitrary units t_{adc} as function of the known values selected in the Delay Unit t_{ns}: $t_{adc} = p0 + p1 \cdot t_{ns}$.

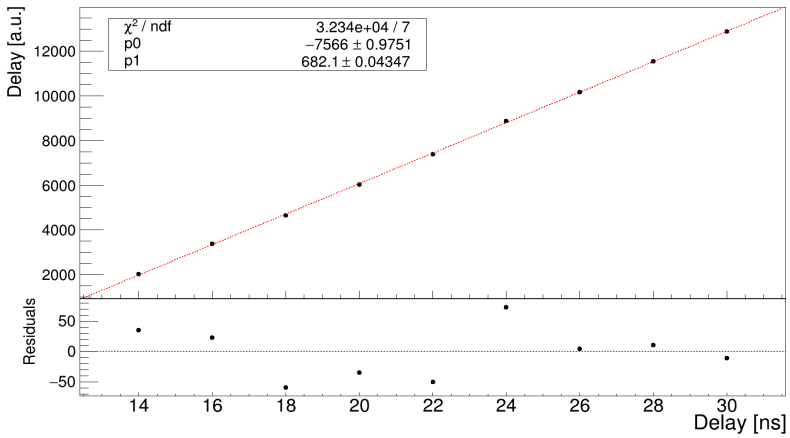

Figure 7: TAC calibration fit.

Delay [ns]	μ [a.u.]	σ [a.u]
14	2019.0	0.7
16	3371.5	0.6
18	4653.6	0.7
20	6041.9	0.7
22	7391.5	0.7
24	8878.3	0.7
26	10174.5	0.7
28	11544.4	0.7
30	12887.2	0.7

Table 2: TAC calibration results.

$$p0 = (-7566 \pm 1)a.u. \qquad p1 = (682.12 \pm 0.04)a.u./ns \tag{4}$$

4.3 Calibration of the delay cables

From the results of the TAC calibration, we have estimated the delay of some LEMO cables that have been subsequently used to optimize the CFTD external delay (Sec. 5.1). To do this, we connected each cable (labeled with letters from A to H and Z), one a time, in series to the one that in the previous part of the experience connected the Delay Unit with the STOP of the TAC. We set for each cable a suitable delay in the Delay Unit in order to see the whole peak (the delay of the cable added to that of the Delay unit must be within the range of [13 ns, 30 ns]). Then we acquired spectra for about 3 minutes and we fitted with Gaussian functions the peak of ch2 to extract the centroid. Using the calibration function (parameters of Eq. 4) we deduced the value of the delay introduced by the cable by subtracting the delay of the Delay Unit to the total delay measured with this procedure.

Cable	A	B	C	D	E
Delay [ns]	1.286 ± 0.004	1.791 ± 0.004	5.190 ± 0.004	1.132 ± 0.004	5.160 ± 0.003
Cable	F	G	H	Z	
Delay [ns]	1.248 ± 0.004	1.125 ± 0.003	2.636 ± 0.003	$5,308 \pm 0.006$	

5 Time resolution optimization

In this section, we want to investigate the dependence of the temporal resolution as a function of different parameters: the external delay of CFTD and the energy of the events analyzed.

5.1 Time resolution as a function of the external delay of CFTD

The temporal resolution depends on the external delay of CFTD which, in this case, can be manually set by using a proper cable. Since the manufacturer attenuation factor F is 20% we need an external delay of about 80% of the rise time (that in this case was $\sim 6ns$): this value corresponds to an external delay of $D \simeq 5ns$. We decided to separately optimize the two CFTDs used (that are labeled as 1 or 2 depending on the detector connected). To do this, we varied the external delay using the calibrated cables (Sec. 4.3). For each configuration we adjusted the WALK ADJ (Z): this was possible by acting on the potentiometer with a screwdriver until the zero crossing dispersion was minimized.
Firstly, we optimized the CFTD1 by keeping as external delay in CFTD2 the expected delay value of $\sim 5ns$ (through the cable Z). Then, by keeping fixed the optimal configuration of CFTD1 (cables H + B), we optimized the CFTD2. It has been measured the FWHM of the temporal distribution, for each external delay, by fitting with a Gaussian the TAC distribution.

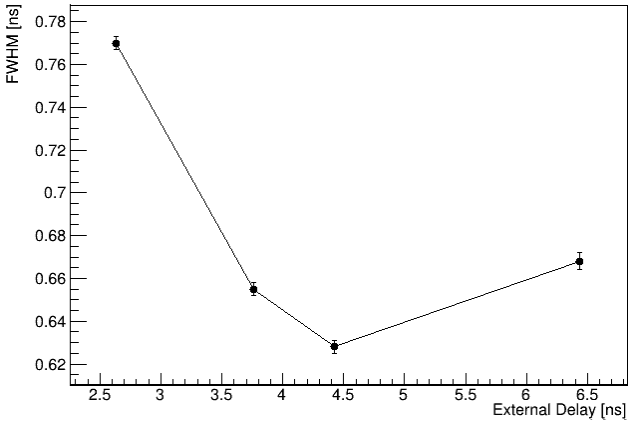

Figure 8: Optimization of CFTD1: FWHM as function of cable external delay.

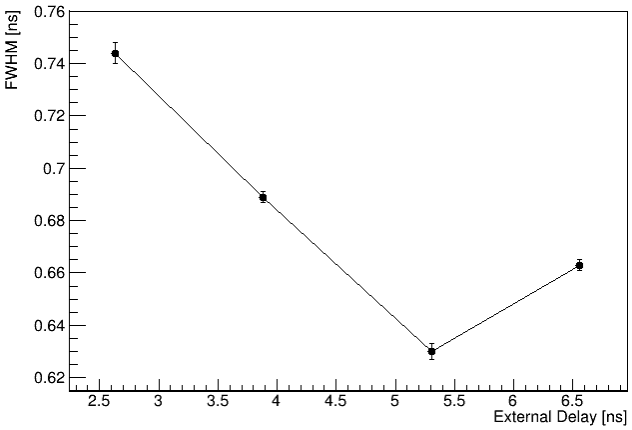

Figure 9: Optimization of CFTD2: FWHM as function of cable external delay.

Cables	External delay [ns]	FWHM [ns]	Cables	External delay [ns]	FWHM [ns]
H	2.636 ± 0.003	0.770 ± 0.003	H	2.636 ± 0.003	0.744 ± 0.004
H+G	3.761 ± 0.004	0.655 ± 0.003	H+F	3.884 ± 0.005	0.689 ± 0.002
H+B	4.427 ± 0.005	0.628 ± 0.003	Z	5.368 ± 0.006	0.630 ± 0.003
C+F	6.438 ± 0.006	0.668 ± 0.004	Z+F	6.557 ± 0.007	0.663 ± 0.002

Table 3: FWHM computed for each external delay of CFTD1 (left) and CFTD2 (right).

5.2 Time resolution as a function of the energy

It is known that the temporal distribution is not exactly Gaussian: this effect is due to the dependence of the CFTD timing resolution on the energy of the incident photons, since the time pick-off can depend on the amplitude of the signals. In this section, we want to analyze the dependence of temporal resolution on the energy to find the best energy range that minimizes the FWHM of the TAC spectrum. To do this, we performed a twenty-hour measurement with a ^{60}Co source, keeping the detectors adjacent to the collimator. The ^{60}Co emits photons with energies of 1.17MeV and 1.33MeV randomly oriented in all directions: unlike ^{22}Na, in this case, it is more difficult to have coincidences (for this reason we acquired the spectrum for all the night). On the other hand, the higher energy photons emitted by the source allow having a spectrum with enough statistics until 1 MeV.
We carried out two analysis in order to see the dependence of the FWHM of the TAC distribution on a lower energy threshold and, more specifically, on the energy ranges of the selected events. As in the previous cases, the FWHM has been measured by using a Gaussian fit of the TAC distribution. We created a macro that selects the events whose energy satisfies some conditions. We started by imposing an energy threshold that varies from $100keV$ up to $1MeV$ (with steps of $50keV$). Then we remade the analysis by imposing the energy of the selected photons within ranges of $100keV$ wide, by analyzing all the values between 50keV and 1150keV (as shown in Tab. 4). The results are shown in Fig 10 and 11. In Fig. 11 we have indicated the different energy ranges used by reporting their mean values.

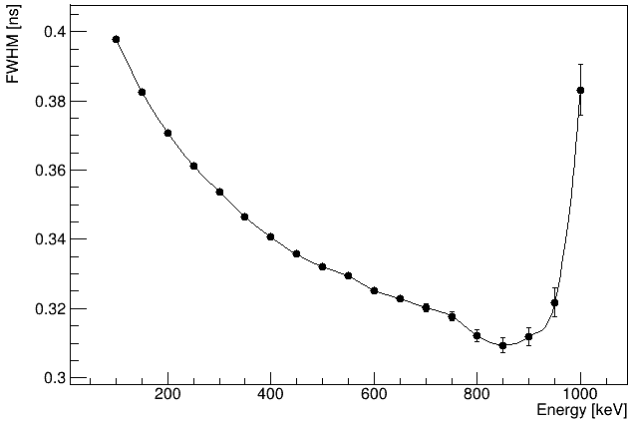

Figure 10: FWHM as function of the lower energy threshold.

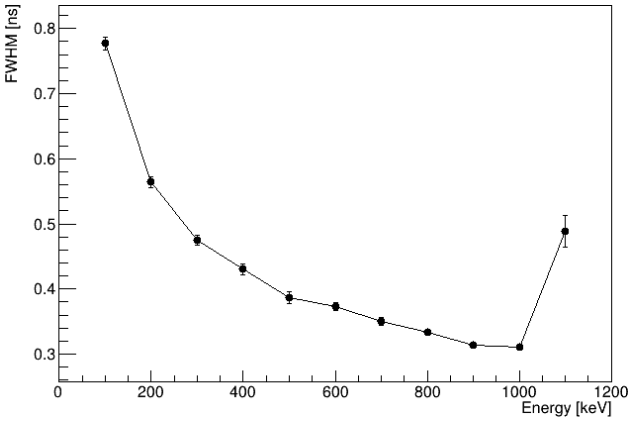

Figure 11: FWHM as function of the energy range.

Lower Threshold [keV]	FWHM [ns]	Lower Threshold [keV]	FWHM [ns]	Range [keV]	FWHM [ns]
100	0.398 ± 0.001	600	0.325 ± 0.001	[50-150]	0.78 ± 0.01
150	0.383 ± 0.001	650	0.323 ± 0.001	[150-250]	0.565 ± 0.008
200	0.371 ± 0.001	700	0.320 ± 0.001	[250-350]	0.475 ± 0.008
250	0.361 ± 0.001	750	0.318 ± 0.001	[350-450]	0.43 ± 0.008
300	0.354 ± 0.001	800	0.312 ± 0.002	[450-550]	0.387 ± 0.009
350	0.346 ± 0.001	850	0.309 ± 0.002	[550-650]	0.372 ± 0.006
400	0.341 ± 0.001	900	0.312 ± 0.003	[650-750]	0.350 ± 0.006
450	0.336 ± 0.001	950	$0,322 \pm 0.004$	[750-850]	0.333 ± 0.005
500	0.332 ± 0.001	1000	0.383 ± 0.007	[850-950]	0.313 ± 0.003
550	0.329 ± 0.001			[950-1050]	0.310 ± 0.004
				[1050-1150]	0.49 ± 0.02

Table 4: FWHM computed for each lower energy threshold (first two columns) and energy ranges (third column).

From both the methods used, we observed that the resolution improves with the increase of the observed energies, obtaining a minimum for a lower threshold of about $850keV$ and for the events within the range $[950keV - 1050keV]$. For energies higher than $1050keV$, the statistics are no longer enough to make an accurate analysis.
We got $(0.309 \pm 0.002)ns$ as the best temporal FWHM for the lower threshold of $850keV$ and in particular we obtained a FWHM of $(0.310 \pm 0.004)ns$ for the energy range of $[950keV - 1050keV]$.

6 Timing analysis through a digital CFTD

The scope of this part of the experiment is to build an algorithm for a digital CFTD and to remake the same analysis (described in Sec. 5.1) to compare the results of the offline analysis with those obtained from the analog chain, based on the CFTD and the TAC. For this scope, we have disconnected the TAC from the digitizer and we have enabled the acquisition of the waveforms on VERDI. Then we acquired for about an hour the coincidence signals of the two detectors related to the source ^{22}Na.

6.1 Optimization of time resolution as a function of F and D

We made an algorithm capable of analyzing the recorded waveforms of each detector to reproduce the same operations of a digital CFTD by varying the external delay D and the attenuation factor F. We summarize the operation of the digital CFTD:

- Each waveform recorded is labeled with a number to identify the coincidence events of both the detectors. The original ROOT file can be read with a specific macro that plots the waveform of a selected event for both the detectors. The first step consists in subtracting the baseline from the signal. A lot of events of the detector D1 presented a sinusoidal baseline so in this case, we implemented a macro that fit the background with a sinusoidal function.

- However, after subtracting the baseline, there were still some spurious signals, so we imposed in the code a filter to select only the events whose baseline did not fluctuate beyond a threshold value of 5 a.u. with respect to zero.

- The selected events have been split: the first has been delayed of a quantity D, instead, the second has been attenuated by a fraction F. The two signals were then added together (see Fig. 13).

- The time reference of the events corresponds to the zero crossing of the bipolar signal. We created a code that finds the two points that are just before and after the zero level respectively, within the range between the absolute minimum and the absolute maximum of the bipolar signal. Then we found the zero crossing point as the intersection of the segment joining these two points and the zero level.

- We obtained the time reference value of each event and the difference of the corresponding times Δt recorded by the two detectors. For each choice of D and F, we made a histogram with the distribution of the quantity Δt and we estimated the FWHM with a Gaussian fit of the peak.

- Finally, we made a two dimensional scan of D and F by varying D in the range [1 ns, 10 ns] (with step-size 1ns, which corresponds to the time unit of the digitizer) and F in [10%, 100%] (with step-size 10%).

From the 2-dimensional plot of FWHM (Fig. 12) as function of D and F and we found the minimum, which corresponds to the optimal configuration:

$$D = 5ns \qquad\qquad F = 10\% \tag{5}$$

These values are similar to those obtained through the analogue CFTD. They have been fixed for the rest of the analysis. Now it is possible to reproduce the same analysis of Sec. 5.1 and to compare the results obtained through the digital CFTD with that obtained from the analogue one.

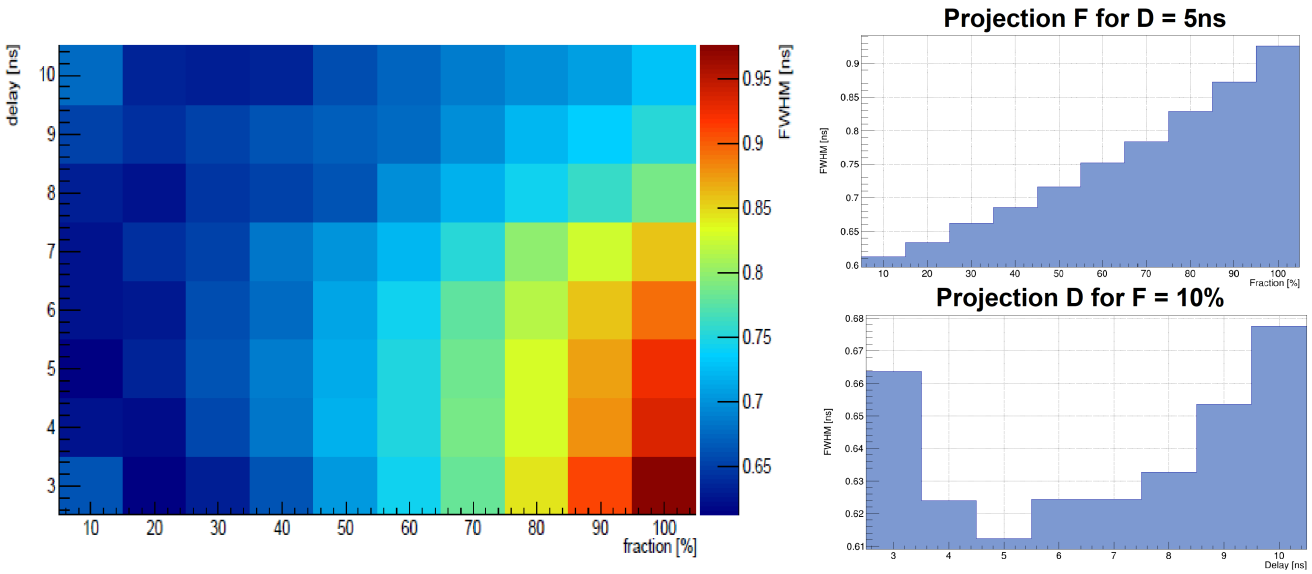

Figure 12: On the left side there is the 2-dimensional scan of D (Delay) and F (fraction). The optimal values that minimize the FWHM are: $D = 5ns$ and $F = 10\%$. On the right side there are two projections of the plot with fixed $D = 5ns$ (top) and fixed $F = 10\%$ (bottom).

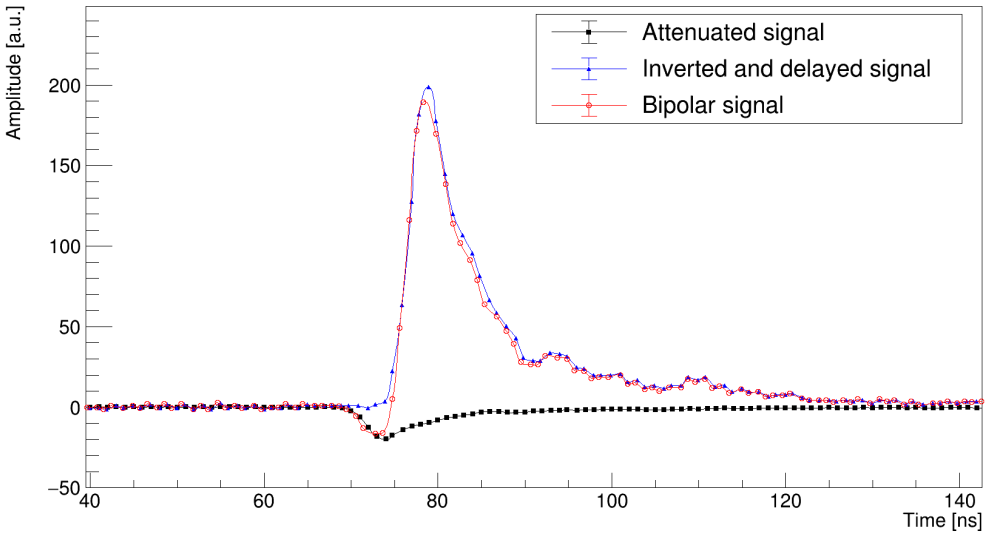

Figure 13: Example of operation of the optimized CFTD on a waveform.

6.2 Time resolution as a function of the external delay of CFTD

We applied the same procedure that is described in Sec. 5.2. The only difference is that here we have used ^{22}Na instead of ^{60}Co and we have acquired it for only one hour. As consequence, we didn't record enough coincidences of photons with energy higher than 350 keV, which is the limit of the right tail of the Compton edge. For this reason, in this analysis, we selected only lower energy thresholds between 50 keV and 300 keV.

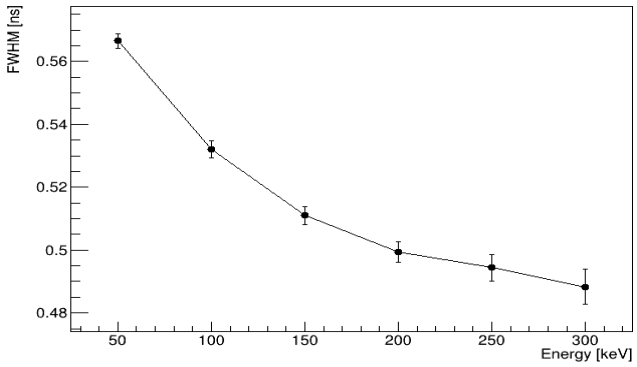

Figure 14: FWHM as function of the lower energy threshold performed through the digital CFTD.

Lower Threshold [keV]	FWHM [ns]
50	0.566 ± 0.002
100	0.532 ± 0.003
150	0.511 ± 0.003
200	0.499 ± 0.003
250	0.494 ± 0.004
300	0.488 ± 0.005

Table 5: FWHM computed for each lower energy threshold.

The FWHM of the temporal distribution obtained through the digital CFTD has a trend similar to that of the analogue chain. If we had used the ^{60}Co (which requires longer acquisition times) we could have identified a precise minimum in a wider range. One interesting difference between the results of the digital and the analogue CFTD is the higher FWHM obtained with the offline analysis. This is probably due to the low energy range to which the events belong: indeed it is possible to see a similar trend in Fig. 11 for energy ranges between 50keV and 300 keV. In Fig. 10 the corresponding lower thresholds allow acquiring also the events with energy around 950keV-1050keV which heavily affect the resolution around the centroid.

6.3 Spectrum obtained from the waveforms analysis

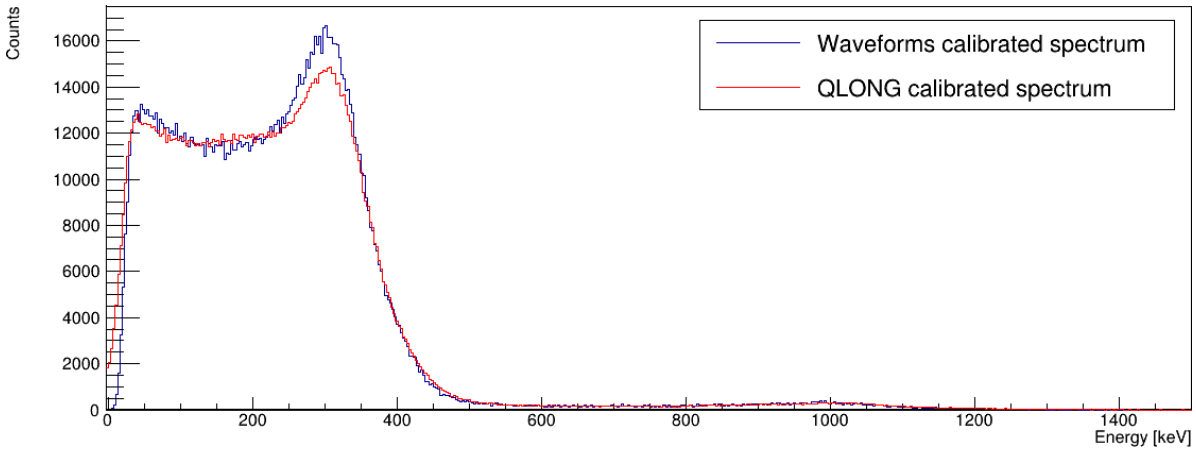

Figure 15: Comparison between the spectrum obtained from the integration of the waveforms and that obtained from QLONG for D1.

The waveforms correspond to the voltage signals of the recorded events (expressed in the arbitrary units of the digitizer). We performed an offline analysis to obtain the energy spectrum based on the waveforms integration. This method consists in integrating each waveform by using rectangles with a base of 1 ns (which coincides with the temporal unit of the digitizer). We applied a digital threshold that accepts only the events over a certain integral value (we set the minimum necessary to select the good signals). The energy, in arbitrary units, is equal to the opposite value of this integral. The spectrum obtained in this way has been approximately calibrated and it has been compared with that obtained from QLONG (Fig. 15).

7 Measurement of the speed of light

In this section it's described the procedure used to estimate the speed of light by exploiting the experimental apparatus and the optimized CFTD external delay. We initially checked that the instrumentation was properly set, in particular, the CFTD parameters such as external delay and WALK ADJ. Then we verified the coincidence system, the width, and the delay of the signals. For this work, the experimental setup has been properly modified (Fig. 16). In particular, the detectors have been placed at the ends of the metallic bar at a fixed distance $d_{D1-D2} = (165.8 \pm 0.1)cm$. The spectra have been acquired for about one hour in two experimental configurations:

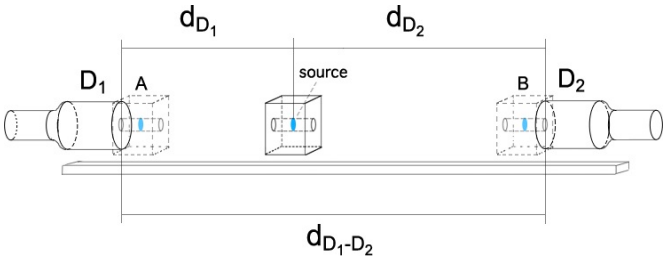

Figure 16: Detectors geometry.

- Configuration 1: Source near the detector D1 at a distance $d_{D1} = (3.7 \pm 0.1)cm$ and $d_{D2} = (162.1 \pm 0.1)cm$ with respect to detector D2.
- Configuration 2: Source near the detector D2 at a distance $d'_{D2} = d_{D1} = (3.7 \pm 0.1)cm$ and $d'_{D1} = d_{D2} = (162.1 \pm 0.1)cm$ with respect to detector D1.

The delay of the Delay Unit has been set to the maximum value of 31.5 ns to visualize, in both the configurations, the whole temporal distributions (the centroid must be higher than 13 ns).
For each calibrated TAC spectrum we performed a Gaussian fit of the peak to estimate the mean delay T of the detected signals [4] (it is called 1 or 2 depending on the analyzed configuration):

$$T_1 = (36.444 \pm 0.004)ns \qquad T_2 = (25.866 \pm 0.004)ns \tag{6}$$

The speed of light can be measured using the following formula:

$$c = \frac{2(d_{D2} - d_{D1})}{T_1 - T_2} \qquad \sigma_c = 2\sqrt{\frac{1}{(T_1 - T_2)^2}(\sigma^2_{d_{D1}} + \sigma^2_{d_{D2}}) + \frac{(d_{D2} - d_{D1})^2}{(T_1 - T_2)^4}(\sigma^2_{T_1} + \sigma^2_{T_2})} \tag{7}$$

$$c = (2.995 \pm 0.004) \cdot 10^8 m/s \tag{8}$$

[4] These Gaussians have been fitted in a suitable range around the centroid in order to correctly find the mean. In the plots these fits have been extended in a larger range.

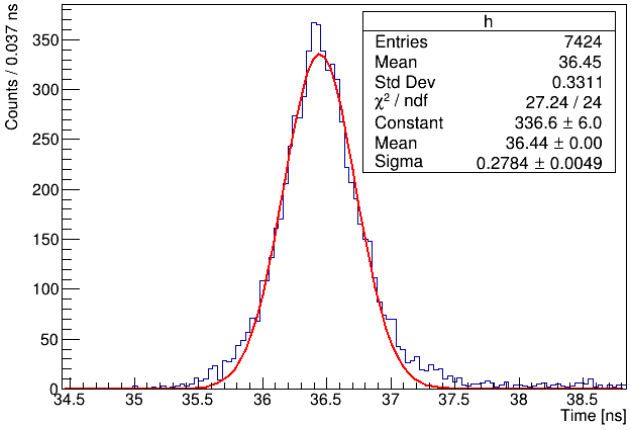

Figure 17: Fitted timing distribution of configuration 1.

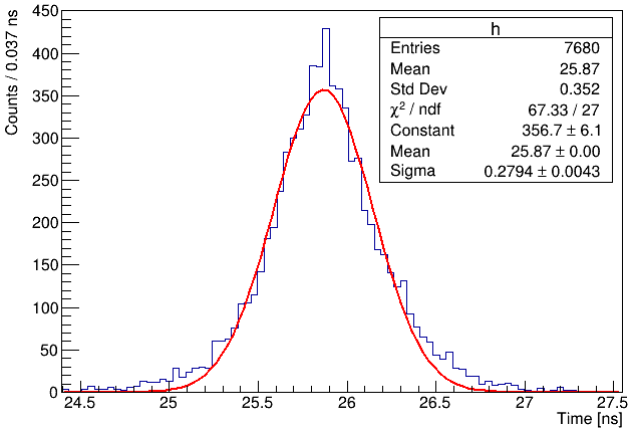

Figure 18: Fitted timing distribution of configuration 2.

This result is a good estimation of the speed of light, compatible with the theoretical value $c_{th} = 2.99792 \cdot 10^8 m/s$. This method turns out to be a good way to estimate the speed of the light since we have demonstrated that most of the systematic errors disappear.
These errors concern:

- The detector positions: we measured the position of the detector by taking as reference value the external endcap. However, a photon typically interacts inside the detector after traveling a mean distance Δs;
- The temporal delay: there are different types of delays between the signals which come from the detectors and the electronics (not only that of the Delay Unit).

These systematic errors disappear by taking the differences $d_{D2} - d_{D1}$ and $T_1 - T_2$ since we can suppose that they affect both measurements in the same way. Therefore, the main contribution to the uncertainty of this estimation is due to the statistical uncertainties of the detector positions and the estimation of the mean delay. Both can be reduced with appropriate choices: the first term can be relatively reduced by increasing the distance between the detectors, instead the second can be reduced by increasing the statistics of the sample.

8 Conclusions and perspectives

In this work, we have optimized the external delay of an analogue CFTD. We have studied the dependence of the timing resolution on the energy of the events recorded. This was possible thanks to the temporal calibration of the TAC and the energy calibration of the detectors. For this last step, we used the method of Gaussian smearing to reproduce the experimental Compton edge: the optimal simulation turned out to be quite similar to the original one.
We reproduced the same analysis also with a digital version of the CFTD and we have found similar results. In particular, we proved that the best choice of delay is $D = 5ns$ and the attenuation fraction $F = 10\%$. In principle, offline analysis is more accurate than the analog one, because it allows scanning all possible combinations of delay and attenuation and it can also select the events that we want to analyze. However, to do this, it requires a lot of computing power. Eventually, the experimental setup has been used to measure the speed of light. We got a good estimation of this well-known physical constant, proving the accuracy of the experimental apparatus.